

Key Points:

- A decade of hourly surface current maps were used to calculate annual and seasonal means along with interannual and intra-annual and seasonal variability
- Mean flows are cross-shore near the coast and southward alongshore with greater speeds offshore
- Wind velocity and river discharge are used to explain the most significant interannual variability

Supporting Information:

- Supporting Information S1

Correspondence to:

H. Roarty,
hroarty@marine.rutgers.edu

Citation:








Roarty, H., Glenn, S., Brodie, J., Nazzaro, L., Smith, M., Handel, E., et al. (2020). Annual and seasonal surface circulation over the Mid-Atlantic Bight Continental Shelf derived from a decade of High Frequency Radar observations. *Journal of Geophysical Research: Oceans*, 125, e2020JC016368. <https://doi.org/10.1029/2020JC016368>

Received 6 MAY 2020

Accepted 6 OCT 2020

Accepted article online 12 OCT 2020

Annual and Seasonal Surface Circulation Over the Mid-Atlantic Bight Continental Shelf Derived From a Decade of High Frequency Radar Observations

Hugh Roarty¹ , Scott Glenn¹, Joseph Brodie¹ , Laura Nazzaro¹, Michael Smith¹, Ethan Handel¹, Josh Kohut¹ , Teresa Updyke² , Larry Atkinson² , William Boicourt³ , Wendell Brown⁴, Harvey Seim⁵, Mike Muglia⁶, Haixing Wang⁷ , and Donglai Gong⁷

¹Center for Ocean Observing Leadership, Rutgers University, New Brunswick, NJ, USA, ²Center for Coastal Physical Oceanography, Old Dominion University, Norfolk, VA, USA, ³Center for Environmental Science, University of Maryland, Cambridge, MD, USA, ⁴School for Marine Science and Technology, University of Massachusetts Dartmouth, New Bedford, MA, USA, ⁵Department of Marine Sciences, University of North Carolina-Chapel Hill, Chapel Hill, NC, USA, ⁶Department of Coastal Studies, East Carolina University, Wanchese, NC, USA, ⁷Virginia Institute of Marine Science, College of William and Mary, Gloucester Point, VA, USA

Abstract A decade (2007–2016) of hourly 6-km-resolution maps of the surface currents across the Mid-Atlantic Bight (MAB) generated by a regional-scale High Frequency Radar network are used to reveal new insights into the spatial patterns of the annual and seasonal mean surface flows. Across the 10-year time series, temporal means and interannual and intra-annual variability are used to quantify the variability of spatial surface current patterns. The 10-year annual mean surface flows are weaker and mostly cross-shelf near the coast, increasing in speed and rotating to more alongshore directions near the shelfbreak, and increasing in speed and rotating to flow off-shelf in the southern MAB. The annual mean surface current pattern is relatively stable year to year compared to the hourly variations within a year. The 10-year seasonal means exhibit similar current patterns, with winter and summer more cross-shore while spring and fall transitions are more alongshore. Fall and winter mean speeds are larger and correspond to when mean winds are stronger and cross-shore. Summer mean currents are weakest and correspond to a time when the mean wind opposes the alongshore flow. Again, intra-annual variability is much greater than interannual, with the fall season exhibiting the most interseasonal variability in the surface current patterns. The extreme fall seasons of 2009 and 2011 are related to extremes in the wind and river discharge events caused by different persistent synoptic meteorological conditions, resulting in more or less rapid fall transitions from stratified summer to well-mixed winter conditions.

Plain Language Summary A coordinated High Frequency Radar network operated between Cape Cod, MA, and Cape Hatteras, NC, generates hourly maps of ocean surface currents. A decade-long study revealed the detailed structure of the surface flows. These flows were compared to wind and river flow data to explain the patterns observed in the flow. Near the coast, the average currents flow offshore. Away from the coast, the average currents flow along the coast toward the south. Fall is the season with the most variability from year to year. Its higher variability can be traced to different regional weather patterns that change the wind fields and the amount of freshwater delivered by the rivers to the coastal ocean. This is the first study to use a decade of observed surface current maps that uniquely and simultaneously observe the changing patterns of the average flow structure along a segment of eastern United States. The improved understanding of the coastal circulation over a wide area, and what drives its variability, has implications for pollutant transport, plankton transport at the base of the food chain, fish and shellfish reproduction, and multiple ocean-based human activities including fishing, marine transportation, and offshore wind energy development.

1. Introduction

The coastal ocean is an intricate system that forms the boundary between the land and the deep ocean. For shallow and wide continental shelves, such as those on the U.S. East Coast, dynamical factors such as

©2020. The Authors.

This is an open access article under the terms of the Creative Commons Attribution License, which permits use, distribution and reproduction in any medium, provided the original work is properly cited.

topography, large-scale circulation, wind, fresh water input, and turbulent dissipation play key roles in governing shelf circulation and dynamics. While the deep ocean experiences independent air-ocean and ocean-benthos interactions, the benthos of the shallow ocean affects the surface layer and in turn the associated along and cross-shelf transport (Soulsby et al., 1993). Wind and buoyancy forcing are critical to the flow and can quickly change the dynamics on time scales ranging from hours and days to seasons and years.

The Middle Atlantic Bight (MAB) supports a complex marine ecosystem, and it has been a focus of coastal oceanographic research since the early 1900s (Bigelow & Sears, 1935). The continental shelf of the MAB extends from Cape Hatteras, NC, in the south to Georges Bank off Cape Cod, MA, in the north. The prominent topographic features in this region are the Hudson Shelf Valley (HSV; Lentz et al., 2014), Nantucket Shoals (Beardsley et al., 1985; Limeburner & Beardsley, 1982), and Great South Channel (Chen et al., 1995). The width of the shelf gradually decreases from ~120 km south of Cape Cod down to ~40 km east of Cape Hatteras. The isobaths are roughly parallel to the coastline except near the HSV and the many shelfbreak canyons distributed throughout the MAB.

Beardsley and Boicourt (1981) present a review of the estuarine and coastal circulation of the MAB. The first dynamical model for the MAB showed a southwest drift of shelf and slope waters from Cape Cod toward Cape Hatteras (Sverdrup et al., 1942). Miller (1952) later showed that there was strong variability about this mean drift in the form of eddies and current filaments. Using arrays of long-term moorings, Lentz (2008) showed that the depth-averaged flow is aligned along the isobaths with the exception of the HSV where the mean flow is shoreward up the shelf valley. Chapman and Beardsley (1989) suggest that the origin of the shelf water is from glacial melt along the southern Greenland coast that propagates south to the MAB as a buoyant coastal current. Beardsley and Winant (1979) show that the southwest flow of this cold glacial water is primarily driven as a boundary current connected to the larger-scale circulation of the western North Atlantic Ocean (Fleming, 2016; Levin et al., 2018; Pringle, 2018).

Technology allowed for more long-term measurements of currents, water temperature and salinity, and meteorological forcing in the 1960s. Beardsley and Boicourt (1981) describe much of the work using these longer time series confirming that transient currents modulate the mean southwest drift. The focus of dynamical research in the 1970s shifted from the mean southwest flow to the current variability. Beardsley et al. (1976) suggest that the current variability of the MAB is mostly wind driven. Moores et al. (1976) show that the wind forcing driving this variability is predominately from the west/northwest except in the summer months when the wind is typically from the southwest. Ou et al. (1981) go on to show observationally that the variability is composed of a wind forced component and a larger-scale free-wave component that is not correlated with the wind and propagates downshelf. Using numerical simulations, Beardsley and Haidvogel (1981) confirm that these current fluctuations do have a local and nonlocal response. The local response is related to local geometry, topography, and forcing while the nonlocal response is due to forcing “distant in time and space.”

Beginning in the late 1990s and early 2000s, High Frequency Radar (HFR) surface current mapping technology was introduced to the region. These networks have supported circulation research in the region including nearshore studies off the coast of New Jersey (Kohut et al., 2004), the response of the shelf water to tropical storms (Kohut et al., 2006), and the seasonal variability of the shelf circulation (Castelao et al., 2008; Dzwonkowski et al., 2009, 2010; Gong et al., 2010). In the MAB, numerous studies have validated the HFR surface currents against more traditional in situ measurements (Haines et al., 2017; Kohut & Glenn, 2003; Kohut et al., 2006, 2012; Ullman & Codiga, 2004) and, as a result, these data now support U.S. Coast Guard Search and Rescue operations in the MAB and throughout the United States (Roarty et al., 2010; Ullman et al., 2006).

Since 2007, the Mid-Atlantic Regional Association Coastal Ocean Observing System (MARACOOS) has operated a regional HFR network consisting of approximately 41 radars. These systems have been maintained through a regional collaboration of eight separate organizations (University of North Carolina [Chapel Hill], Center for Innovative Technology, Old Dominion University, Rutgers University, University of Connecticut, University of Rhode Island, University of Massachusetts [Dartmouth], and Woods Hole Oceanographic Institution). The network provides hourly measurements of ocean surface currents (i.e., representative of water depths of 0.3–2.5 m) within ~250 km of the coast, over an area encompassing more than 190,000 km² of the ocean’s surface, at resolutions of 1, 2, and 6 km. In this study, we focus on

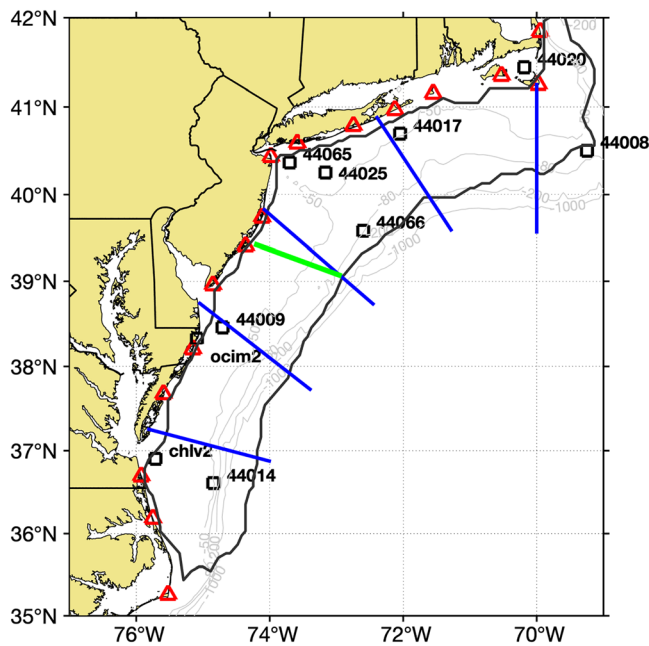


Figure 1. Map of the Mid-Atlantic Bight from Cape Hatteras, NC, up to Cape Cod, MA. The locations of the 5-MHz HF radar stations are denoted as red triangles. NOAA NDBC stations are marked as black squares and labeled. The 50-, 80-, 200-, and 1,000-m isobaths are marked along with the 50% total vector coverage for the study period shown as the thick black line. The Tuckerton endurance line is marked in green. The continental shelf was divided into six regions following definitions used by Wallace et al. (2018). From north to south, the regions are Eastern New England (ENE), Southern New England (SNE), New York Bight 1 (NYB1), New York Bight 2 (NYB2), Southern Shelf 1 (SS1), and Southern Shelf 2 (SS2).

10 years of shelf-wide surface current data provided by this network to examine the response of the surface current fields to local wind forcing and river input over seasonal to annual time scales. The study utilizes wind measurements from several coastal and at-sea wind sensors and river discharge data to describe the response of the two-dimensional structure of the ocean surface flow to these drivers and place that response in the context of atmospheric and oceanic flow features. The paper is divided into the following sections. In section 2, we describe the methods used to collect and process the MARACOOS surface current data set, the National Oceanic and Atmospheric Administration (NOAA) weather buoy and Coastal-Marine Automated Network (C-MAN) station wind data, and the U.S. Geological Service (USGS) river discharge data. In section 3, we characterize the mean and variability of the surface flow, the mean wind over the area, and the seasonality of the surface currents. In section 4, we will discuss the results and draw conclusions in section 5.

2. Methods and Data

2.1. Surface Currents

Surface current measurements were collected in the MAB from 2007 to 2016 using data from sixteen 5 MHz SeaSondes manufactured by CODAR Ocean Sensors (Figure 1). The SeaSonde is a HFR that uses the Doppler shift of radio signals reflected off ocean surface wind waves to measure the component of the ocean current along a radial line toward or away from the station. The average depth of the measurement varies with radar frequency and is proportional to $\lambda/8\pi$, where λ is the radar wavelength (60 m at a 5 MHz transmit frequency). This equates to an average depth measurement of 2.7 m (Paduan & Graber, 1997; Stewart & Joy, 1974). The 60-m radio waves are resonant with ocean waves having a wavelength of 30 m, which equate to waves with a period of 4.3 s in deep water. Each HFR station generated 3-hr-averaged radial component velocity maps every hour; the data collection period for each hourly file was the file timestamp ± 90 min. Each radar utilized a 1-Hz sweep rate for the radio signal and a 1,024-point fast Fourier transform (FFT) for the Doppler processing. This resulted in a radial velocity resolution of approximately ± 1.5 cm/s for each hourly radial vector map.

The hourly radial files were combined into hourly total surface currents using the optimal interpolation scheme (Kim et al., 2008; Kohut et al., 2012). The optimal interpolation parameters used for the total combination were $420 \text{ cm}^2/\text{s}^2$ for signal variance and $66 \text{ cm}^2/\text{s}^2$ for error variance. The radials were weighted based on an exponential decay defined by the decorrelation scales in the north (S_y) and east (S_x) directions. The decorrelation scales in the MAB are larger along the isobaths (Beardsley & Boicourt, 1981; Kohut et al., 2004), so S_y (25 km) was set to 2.5 times that of S_x (10 km) and rotated along isobath. This processing is similar to that utilized in the Kohut et al. (2012) study. Total surface currents were computed on the 6-km national HFR grid (Terrill et al., 2006). For each year of surface current data from December 2006 through November 2016, the `t_tide` toolbox in MATLAB (Pawlowicz et al., 2002) was used to detide data in annual segments (1 December to 30 November; Gong et al., 2010). A 30-hr low-pass filter was then applied to the detided data in order to remove any remaining high-frequency variability. Only grid points with at least 50% coverage (Gong et al., 2010) at a normalized uncertainty level under 0.6 (Kohut et al., 2012) in both the u and v components over the year were included in this analysis. All means, variance, and root mean square (RMS) described below are calculated using the detided and low-pass filtered data that met these quality criteria.

Single-year seasonal means (winter: 1 December to 29 February; spring: 1 March to 31 May; summer: 1 June to 31 August; autumn: 1 September to 30 November) were created by averaging the hourly data over the 3-month period wherever the temporal coverage was at least 50%; annual means were calculated with all hourly data over the 12-month period from 1 December to 30 November, since it had already passed the 50% temporal coverage criterion. Decadal means for each season and for the full year were calculated by

Table 1
List of River Discharges That Were Utilized in the Study

Major River	Minor River	Location	USGS Station No.
Connecticut Hudson		Thompsonville, CT	01184000
		Fort Edwards, NY	01327750
	Mohawk	Cohoes, NY	01357500
	Passaic	Little Falls, NJ	01389500
Delaware Chesapeake	Raritan	Bound Brook, NJ	01403060
		Trenton, NJ	01463500
	Susquehanna	Conowingo, MD	01578310
	Potomac	Washington, DC	01646500
	Patuxet	Laurel, MD	01592500
	Rappahannock	Fredericksburg, VA	01668000
	Choptank	Greensboro, MD	01491000
	James	Cartersville, VA	02035000
	Appomattox	Matoaca, VA	02041650
	Pamunkey	Hanover, VA	01673000
	Mattaponi	Beulahville, VA	01674500

Note. The Hudson and Chesapeake were an amalgamation of several rivers.

taking the mean of all 10 previously calculated means, so each year was weighted equally. Each grid point had to contain at least five individual yearly means (i.e., 50% coverage) to be included in the decadal mean.

For each single-year seasonal and annual mean, a corresponding within-year variance was calculated for both eastward and northward velocities using the hourly surface current data. The decadal seasonal and total intra-annual variance was calculated by taking the mean of the 10 individual-year seasonal and total variances. The interannual variance was calculated by taking the variance of the eastward and northward components of the 10 individual-year seasonal and annual mean current fields. For each within- and between-year variance estimate, a corresponding RMS value was calculated by taking the square root of the sum of the eastward and northward variance values; this RMS considers variation in both current speed and current direction. The same 50% coverage requirements applied to the mean currents were also used for variance and RMS.

The confidence interval of the surface currents on the continental shelf was computed for the decadal mean as well as the seasonal means on the continental shelf following Thomson and Emery (2014). The 95% confidence interval was calculated using the equation $1.96\sigma/(N^*)^{1/2}$, where σ is the standard deviation and N^* is the effective degrees of freedom. N^* was calculated using this equation, $N^* = N\Delta t/T$, where N is the number of samples, Δt is the sampling interval (1 hr), and T is the integral time scale. T was calculated to be 19 hr from a year's worth of data at midshelf offshore of New Jersey; hence, N^* was 4,870 for the decade of data and was 1,218 for each of the seasons. The uncertainty amounted to ± 0.2 – 0.6 cm/s for the decadal mean and within ± 0.4 – 1.0 cm/s for the seasonal means.

confidence interval was calculated using the equation $1.96\sigma/(N^*)^{1/2}$, where σ is the standard deviation and N^* is the effective degrees of freedom. N^* was calculated using this equation, $N^* = N\Delta t/T$, where N is the number of samples, Δt is the sampling interval (1 hr), and T is the integral time scale. T was calculated to be 19 hr from a year's worth of data at midshelf offshore of New Jersey; hence, N^* was 4,870 for the decade of data and was 1,218 for each of the seasons. The uncertainty amounted to ± 0.2 – 0.6 cm/s for the decadal mean and within ± 0.4 – 1.0 cm/s for the seasonal means.

2.2. Winds

Wind data from 10 NOAA National Data Buoy Center (NDBC) stations (44008, 44009, 44014, 44017, 44020, 44025, 44065, 44066, chl2, and ocim2) were used for the wind analysis. Hourly wind data over the 10-year record from 2007 to 2016 were accessed online (<https://www.ndbc.noaa.gov>). A minimum of 50% temporal coverage was required of the annual or seasonal record to be included in the analysis. The wind data were averaged in the same manner as the current data to generate the seasonal means. The statistics of the wind speed and direction were performed by converting wind speed and direction into an east and north vector; all the east vectors were averaged, and all the north vectors were averaged, and then the resulting two vectors were combined to obtain a mean wind vector. The wind velocity data were then converted to wind stress using the wind stress function found in the Climate Data Toolbox for MATLAB (Greene et al., 2019).

2.3. River Discharge

Daily river discharge data were collected from the U.S. Geological Survey (USGS) water data available online (<http://waterdata.usgs.gov/nwis>) for the Connecticut and Delaware rivers. Discharge data from the Hudson, Mohawk, Passaic, and Raritan rivers were combined into a single product and labeled the Hudson River. Discharge data from the Susquehanna, Potomac, Patuxent, Rappahannock, Choptank, James, Appomattox, Pamunkey, and Mattaponi rivers were combined into a single data set and labeled the Chesapeake. The USGS station number corresponding to each river is given in Table 1. The discharge data from the individual stations were merged following the methodology of Chant et al. (2008) and Zhang et al. (2009). The final discharge data sets are made available on the Rutgers ERDDAP server (http://tds.marine.rutgers.edu/erddap/tabledap/ROMS_DISCHARGE.graph). The yearly and seasonal mean and standard deviation of river discharge data are provided in Table 2.

3. Results

3.1. Decadal Mean Surface Currents

Throughout the manuscript, wind direction will follow the meteorological convention where direction indicates where the wind is blowing from and the currents will be described in the oceanographic convention

Table 2
Annual and Seasonal Mean River Discharge Along With One Standard Deviation

	Annual		Winter		Spring		Summer		Fall	
	Mean	$\pm s$	Mean	$\pm s$	Mean	$\pm s$	Mean	$\pm s$	Mean	$\pm s$
Connecticut	675	551	659	378	1,096	611	485	337	457	301
Delaware	630	626	704	417	884	579	449	290	447	337
Hudson	770	629	855	395	1,165	692	538	389	557	346
Chesapeake	2,524	2,521	3,073	1,865	4,242	2,322	1,311	728	1,483	1,276

where direction indicates where the current is flowing toward. The wind field as observed by the 10 wind sensors in the region shows a mean wind from the west northwest that increases speed with distance offshore and rotates slightly to be out of the northwest near the shelfbreak (Figure 2a). Wind variability is denoted by ellipses that represent two standard deviations in the data shown with a scale of 15 m/s. The mean surface flow over the 10-year period (2007–2016) as measured by the MARACOOS long-range HF radar network was offshore and equatorward with a speed of 2–12 cm/s (Figure 2b) with the mean across the entire field of 7 cm/s. The alongshelf currents increase with increasing water depth, consistent with Lentz (2008). Compared to the mean, the currents are most steady along the shelfbreak and most varied near the coastline, essentially varying in offshore direction in concert with the change in coastline orientation. North of the HSV, the currents are toward the southwest while south of the HSV the currents are toward the southeast rotating clockwise toward the southwest with distance offshore. This agrees with

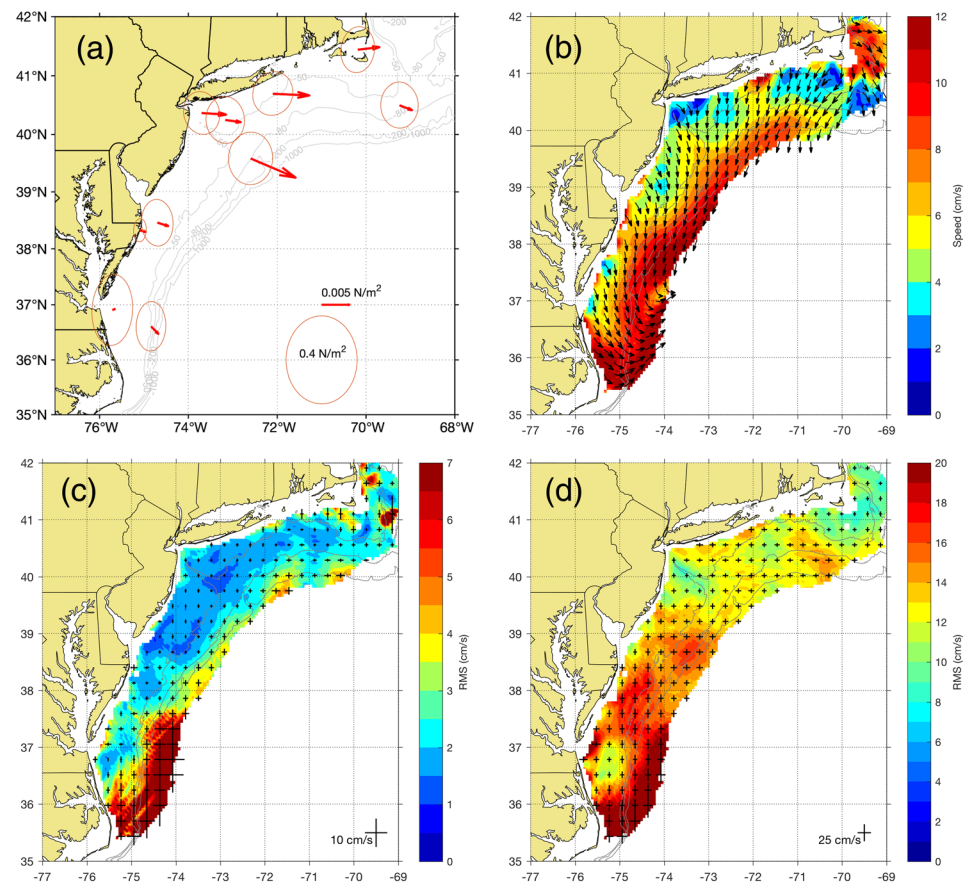


Figure 2. (a) Mean and 95% data ellipse of wind stress (N/m^2) from NDBC stations for 2007–2016. The reference vector of 0.005 and $0.4 N/m^2$ variability ellipse is given in the lower right. (b) Mean surface current for the Mid-Atlantic Bight (cm/s) colorbar indicates magnitude and vectors indicate direction toward of surface current. (c) Interannual standard deviation of the surface currents (cm/s). (d) Intra-annual standard deviation of the surface currents (cm/s).

the earlier work by Gong et al. (2010), who observed the HSV divides the flow into two regimes north and south of the valley. The currents gradually transition from SE to SW with increasing depth; southward currents are centered along the 50-m isobath from Virginia to New Jersey. The surface currents strengthen seaward of the 50-m isobath with speed increasing to 7–11 cm/s with faster flow observed further south. South of the Chesapeake Bay (CB), the flow then turns offshore and merges with the Gulf Stream. The broad band of fast flowing current over the outershelf and shelfbreak is persistent throughout most of the year, and it is thought to be associated with the meandering shelfbreak jet (Linder & Gawarkiewicz, 1998). However, other factors such as buoyancy-driven flow from the rivers also likely contributed to this enhanced flow feature. For our purpose, we will continue to call it the shelfbreak jet, but please keep in mind that this is only in a statistical sense. Any synoptic realization of the shelfbreak jet will likely look very different than this average view.

The surface flow east of Cape Cod is predominantly to the southeast. Below Cape Cod, the flow turns toward the southwest to join the flow south of Rhode Island. Moving south from Cape Cod, the mean surface flow is along isobath toward the equator, consistent with previous studies that analyzed the depth-averaged flow with current meters (Beardsley & Boicourt, 1981; Lentz, 2008) and HF radar (Gong et al., 2010).

The weakest flow regions are observed near the New York Bight apex and south of Cape Cod where the surface currents drop to between 1 and 3 cm/s. The strongest flows in the region are observed near the Gulf Stream, east of Cape Cod, and Nantucket and a strong coastal current along the coast of North Carolina (Lentz et al., 2003).

The influence of the rivers can be seen as the increased velocity regions near the eastern end of Long Island, south of the HSV, south of the Delaware Bay (DB), and the strengthened coastal current along the coast of North Carolina off of the Chesapeake.

3.2. Variability of Surface Currents

The variability of the surface current is significant compared to the mean. The standard deviation within a year (Figure 2) is between 10 and 20 cm/s for the entire field reaching a peak of 20 cm/s off Cape Hatteras where the variability in the position of the Gulf Stream factors significantly (Andres, 2016). Marks representing one standard deviation in the east/west and north/south direction for every fifth grid point are shown with a reference of 25 cm/s in the lower right of the figure. The average standard deviation for the entire field is 15 cm/s. The standard deviation in the northern portion of the domain is of the order 10 cm/s and gradually increases to 20 cm/s in the southern portion of the domain. While the climatological mean is toward the equator, the daily mean can be poleward or opposite the mean flow for several days if the wind conditions are from the south or southwest (Bumpus, 1969; Frey, 1978). Two regions of lower variability are seen over the New Jersey shelf and off the Virginia/North Carolina coast.

The variability from year to year is much less than the variability within the year. The average variability between years is 4 cm/s for the entirety of the domain (Figure 2c). Marks representing one standard deviation in the zonal and meridional direction for every fifth grid point are shown with a reference of 10 cm/s in the lower right of the figure. The variability between years increases across the shelf most likely due to the position of the shelfbreak jet (Fratantoni & Pickart, 2003; Linder & Gawarkiewicz, 1998). The variability between years is highest in the southern region extending up to 37.5°N latitude where the location of the Gulf Stream may influence this variability.

3.3. Seasonal Mean Flow

The surface current and wind data were seasonally averaged following Flagg et al.'s (2006) climatological analysis of the subsurface currents on the outer shelf and Gong et al.'s (2010) analysis of the surface currents on the shelf. The following is a discussion of the seasonally averaged winds (Figure 3) and currents (Figure 4). Again, the variability in the wind is denoted by ellipses that represent two standard deviations in the data. The variability of the wind is two to three times the mean in the MAB, which is reflected in the surface currents. Note that the maps of the seasonal winds and currents are arranged with winter in the upper left and progressing clockwise through the seasons to make it easier for the reader to identify the season-to-season changes in adjacent maps.

To describe the regional differences in surface transport, the continental shelf off the northeast United States is divided into four distinct regions, by combining some of the same regional definitions used by Wallace et al. (2018) in their hydrographic analysis. From north to south, the four analysis regions are Region 1

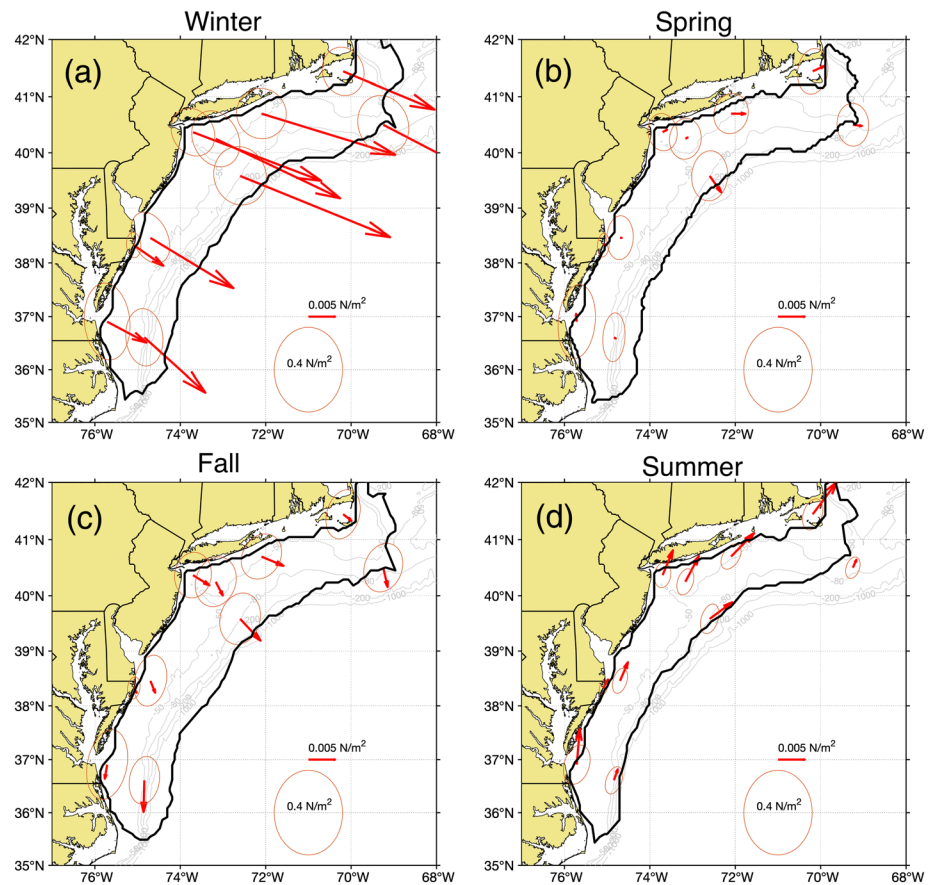


Figure 3. Map of mean and two standard deviation data ellipse of wind stress by season (a) winter, December–February; (b) spring, March–May; (c) fall, September–November; and (d) summer, June–August. The reference vector of 0.005 and 0.4 N/m^2 variability ellipse is given in the lower right of each figure. The 50% total vector coverage boundary for each season is shown as the thick black line.

encompassing Eastern New England (ENE), Region 2 encompassing Southern New England (SNE) and New York Bight 1 (NYB1), Region 3 encompassing New York Bight 2 (NYB2) and Southern Shelf 1 (SS1), and Region 4 encompassing Southern Shelf 2 (SS2). In addition, we defined the MAB region as encompassing the three southernmost regions (similar to the regions defined by Mountain, 2003, but modified to better encompass the inner-shelf domains). These regions are illustrated in Figure 1. We focused the wind analysis on four stations as being representative of the wind field within the particular regions: Region 1 (44008), Region 2 (44025), Region 3 (44009), and Region 4 (44014).

The seasonal maps of the 10-year average HFR surface current and NOAA buoy winds reveal the following:

Winter: From December to February, strong winds from the west-northwest are present over the entire area (Figure 3a), and the flow is similar to the long-term mean (Figure 4a). The ocean surface currents are predominantly offshore, only slightly to the right of the winds with peak velocities between 7 and 12 cm/s. The core of the shelfbreak jet has moved offshore to over the 1,000-m isobath. The current response was divided into four subregions, which allows for a finer description of the flow (Figure 1). (1) ENE: Flow to the east over Nantucket Shoals diverges to east and south. (2) SNE and NYB1: Currents are toward the south on inner shelf turning to the south southwest as they cross the shelfbreak. The low current area south of Nantucket has slightly increased speeds compared to the decadal mean, and currents are directed much more to the south. (3) NYB2 and SS1: Currents are offshore toward the southeast over the inner shelf turning south as they cross the shelfbreak. And lastly, Region (4) SS2: Currents are alongshelf turning counterclockwise to transport water off of the shelf into the Gulf Stream.

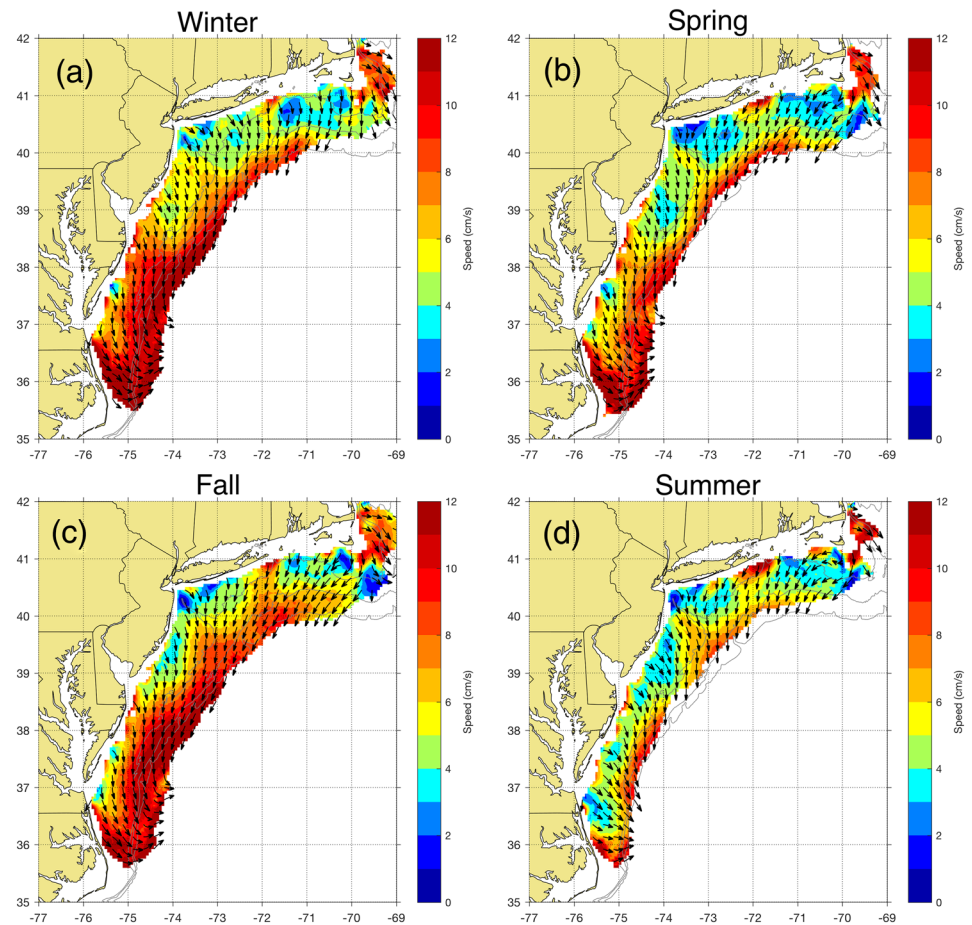


Figure 4. Mean surface currents (2007–2016) by season (a) winter, December–February; (b) spring, March–May; (c) fall, September–November; and (d) summer, June–August. Colorbar indicates magnitude (cm/s) and vectors indicate direction toward of surface current.

Spring: From March to May, weak winds from the west are present nearshore (Figure 3b) with slightly stronger winds in the eastern portion of the domain. The currents inshore of the 100-m isobath are weaker than winter with velocities of 3–6 cm/s. Stronger alongshore currents persist offshore of the 100-m isobath in the range of 9–12 cm/s (Figure 4b). There is a distinct continuous shelfbreak jet, with a wide peak that starts south of Martha’s Vineyard and runs continuously until it turns offshore before reaching Cape Hatteras. (1) ENE: Again, currents are to the southeast and south to the right of the wind are observed. (2) SNE and NYB1: Currents are to south southwest over most of the shelf with south and south-southeast currents near the HSV. South of Nantucket, there are weak currents to the southwest, opposite of the wind. (3) NYB2 and SS1: currents to the southeast over inner shelf, turning to southwest over outer shelf. (4) SS2: Outflow hugs the coastline, turns with the coast, and is then transported offshore into the Gulf Stream. There is a pathway from the shelf/slope front to the east into the Gulf Stream as far north as CB.

Summer: From June to August, the winds are at the midrange of speeds (1.0 to 1.9 m/s) and from the southwest (Figure 3d), typical of the large-scale response to the summer Bermuda high (Zhu & Liang, 2013). Summer has the weakest flows of all the seasons with currents of 3–6 cm/s over most of the shelf (Figure 4d). The currents along the 100-m isobath are slightly faster than those inshore of that isobath. Currents are predominantly offshore, about 90° to the right of the winds in this highly stratified season with peak velocities, 6–8 cm/s, over the 100-m isobath. (1) ENE: There is an area of weak currents and divergence southeast of Nantucket. North of this, there are strong currents to the southeast. (2) SNE and NYB1: Currents are south-southwest over most of the shelf. South of Nantucket and Martha’s Vineyard, there are weak west to southwest flows, and a small area south of Nantucket has northwest to north-northwest

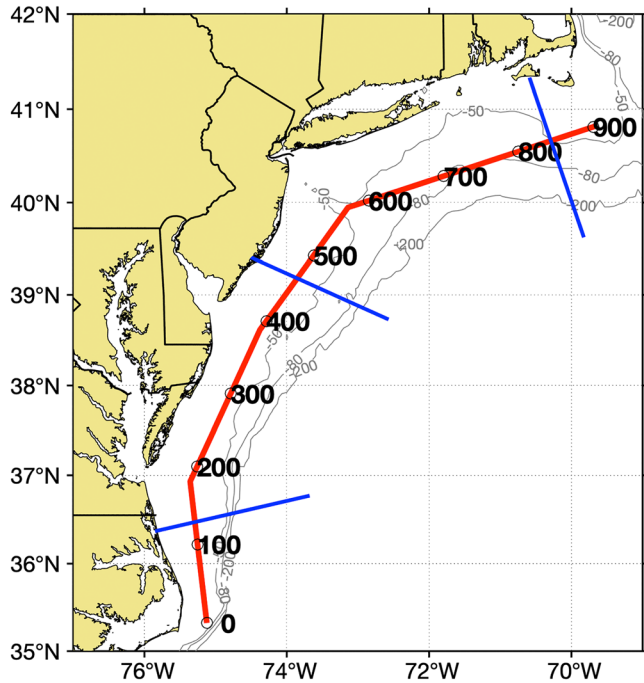


Figure 5. Reference line along the midshelf (red) used to calculate the cross-shelf and alongshelf flow along the Mid-Atlantic Bight. The numbers represent distance in kilometers along the reference line from south to north. The blue lines are the cross section lines that are shown in Figure 7.

flow that is not present in any other season. Strong flows from Long Island and Block Island Sounds are offshore to the southwest. (3) NYB2 and SS1: The cross-shelf flow extends further out over the shelf before turning more alongshore, and the inner-shelf flow is weaker than in other seasons. (4) SS2: weaker flow and directed more cross-shelf than in the other seasons, transporting water to the southeast off the shelf toward the Gulf Stream.

Fall: From September to November, it has similar medium wind speeds as summer but turned to be from the northwest, in the offshore direction (Figure 3c). Fall displays the fastest currents of all the seasons with currents greater than 6 cm/s over most of the shelf (Figure 4c). Compared to summer, the currents across most of the shelf increase in speed, especially off Maryland and Virginia where they accelerate to 13 cm/s along the 80-m isobath. The shelfbreak jet is the strongest and widest in fall with peak currents beginning south of Martha's Vineyard. The broad peak extends between the 60- and >1,000-m isobaths. This feature flows all the way south to join the Chesapeake outflow and flow offshore to the Gulf Stream in one wide region. (1) ENE: The flow is to east over Nantucket Shoals. Southeast of Nantucket, there are slower currents directed to the southeast. (2) SNE and NYB1: South-southwest currents on the inner shelf turn slightly to the southwest over the outer shelf, accelerating in the alongshelf direction. (3) NYB2 and SS1: On the inner shelf the currents are offshore and toward the south, turning to alongshelf over the middle to outer shelf. At the outer shelf and in the slope water the currents are alongshelf, 90° to the right of wind. (4) SS2: Outflow along the coast is strong and joins the shelfbreak jet over the shelf and both flow offshore in one current

The seasonal mean and standard deviation of the discharge (m^3/s) for each of the four major rivers in the MAB are shown as Table 2. The outflows from the Connecticut, Delaware, and Hudson are of the same order

while the outflow from the Chesapeake is two to four times larger than each of these rivers. The freshwater outflow analysis is from the four major rivers within the Mid-Atlantic and not fresh water from the Gulf of Maine. The largest outflow is in the spring accounting for 40% of the fresh water into the system with the lowest discharge in the summer only accounting for 15%. This pattern also holds true for the variability with the spring accounting for 21% of the variability (one standard deviation) and the summer accounting for only 6% of the variability.

3.4. Alongshelf and Cross-Shelf Flows

In this section a quantitative description of the seasonal flow in the MAB is provided. The alongshore and cross-shore current was calculated over a midshelf line (Figure 5a), and the distance in kilometers along the line is overlaid on the line where the origin is east of Cape Hatteras and increases toward the north. The bearing along this line was used to rotate the surface currents into an alongshelf and cross-shelf coordinate system. The new current components were then plotted as a function of distance along the isobath as shown in Figure 6a for the alongshelf flow and Figure 6b for the cross-shore flow. The approximate location of where the four major estuaries connect to the shelf water are drawn as horizontal lines in Figure 6, CB at distance marker 150 km, DB at 350 km, Hudson River at 550 km, and Long Island Sound (LIS) at 700 km.

Three distinct regions emerge from these plots. The first region from 0 to 150 km is where the shelf slope front turns offshore and the CB plume accelerates along the coast, and the two flows join with the Gulf Stream to be advected to the northeast. Within this region there is an increase in both the alongshelf flow and cross-shelf flow. The cross-shelf flows are consistent from season to season. Winter and fall display the greatest alongshelf flow while summer exhibits the weakest alongshelf flow. Spring resides in the middle with an alongshelf flow of 4 cm/s near CB accelerating to 9 cm/s near Cape Hatteras.

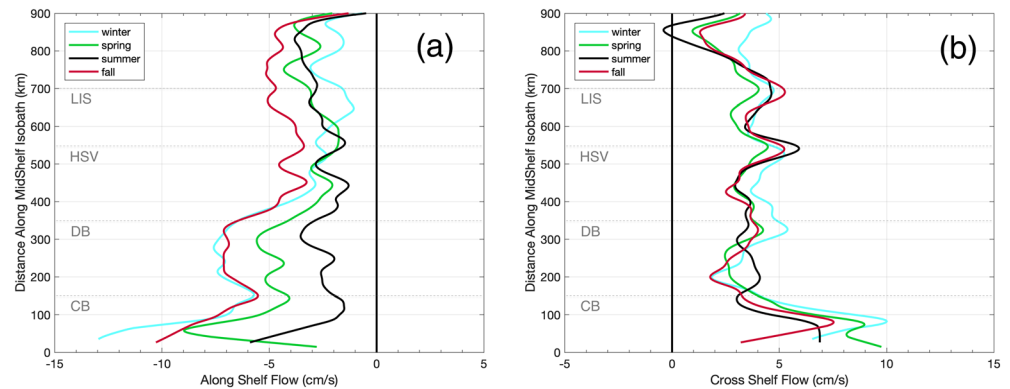


Figure 6. (a) Alongshelf current plotted by distance along the midshelf line (Figure 5a) by season winter (blue), spring (green), summer (black), and fall (red). (b) Cross-shelf current plotted by distance along the midshelf line. The locations of the four major estuaries are denoted by the dotted lines Long Island Sound (LIS), Hudson Shelf Valley (HSV), Delaware Bay (DB), and Chesapeake Bay (CB).

In the middle region between 150 and 800 km shows a consistent alongshelf flow from 800 to 350 km near DB and then an increase in alongshelf flow south of this location during some seasons. The alongshelf flow is strongest in the fall and weakest in the summer. The cross-shelf flow is offshore for each season, and the alongshelf flow is equatorward in each season. The cross-shelf flow is consistent between the seasons. There are local maximum points in the cross-shelf flow near the major estuaries at LIS, HSV and DB. The cross-shelf flow then accelerates when it reaches CB at 150 km. South of the 350-km distance marker, there is an increase in the alongshelf flow except in summer. It is in this middle zone where all the variation in space and seasonality takes place. In winter when the water column is well mixed, the flow will be more influenced by topography while in the summer it will be influenced by the stratification. Lastly, the region from 800 to 900 km exhibits an alongshelf flow that is consistent between the four seasons. The cross-shelf flow is 1–4 cm/s while winter exhibits the strongest cross-shore flow due to the strong winds from the northwest.

The findings for distances 0–800 km along the midshelf line show a stronger cross-shelf flow than measured by Lentz (2008), who found the cross-shelf flow to be between 1 and 3 cm/s near the surface. This is understandable, as the Lentz near-surface velocities were from the shallowest measurement of an acoustic current meter within 20 m of the surface while the HFR measurement is within 3 m of the surface. Any shear in the water column would explain these differences. Lentz (2008) also noted that the current meter records showed stronger offshore flows in the northern MAB and weaker cross-shelf flows in the southern MAB. This agrees for the area off Cape Cod. We note an area of increased cross-shelf flow off of Cape Hatteras.

Next, cross sections were taken through the seasonal flows to look at the variability of the along and cross-shelf flow in relation to their location within the MAB. Figure 7 shows the alongshelf velocity (top panel), cross-shelf velocity (middle panel), and water depth (lower panel) for the three cross sections (blue lines) from Figure 5. The three cross sections fall within three of the subregions Southern Shelf 2 (SS2), New York Bight 2 (NYB2), and Southern New England (SNE), which can be thought of as the entrance, middle, and exit of the flow through the MAB, respectively. The alongshelf and cross-shelf flow are plotted against distance offshore (km). Positive alongshelf flow is toward the northeast, and positive cross-shelf flow is offshore. The largest seasonal variability at the entrance (Region SS2) to the MAB is displayed in the alongshelf current while the exit (Region SNE) exhibits the strongest seasonal variability in the cross-shelf. The seasonal variability in the middle of the MAB (Region NYB2) is at a minimum, which is in contrast to the highly variable winds in each season as shown in Figure 3. This suggests that the mean alongshelf flow is not influenced by the wind but is driven by a large-scale alongshelf pressure gradient (Lentz, 2008). Each of the cross sections display a coastal current that is toward the equator and an increasing alongshelf flow with distance offshore. Region NYB2 displays a linearly increasing alongshelf flow while Region SS2 reaches a maximum alongshelf flow at 120 km offshore just past the shelfbreak and then transitions to cross-shelf flow in the vicinity of the Gulf Stream.

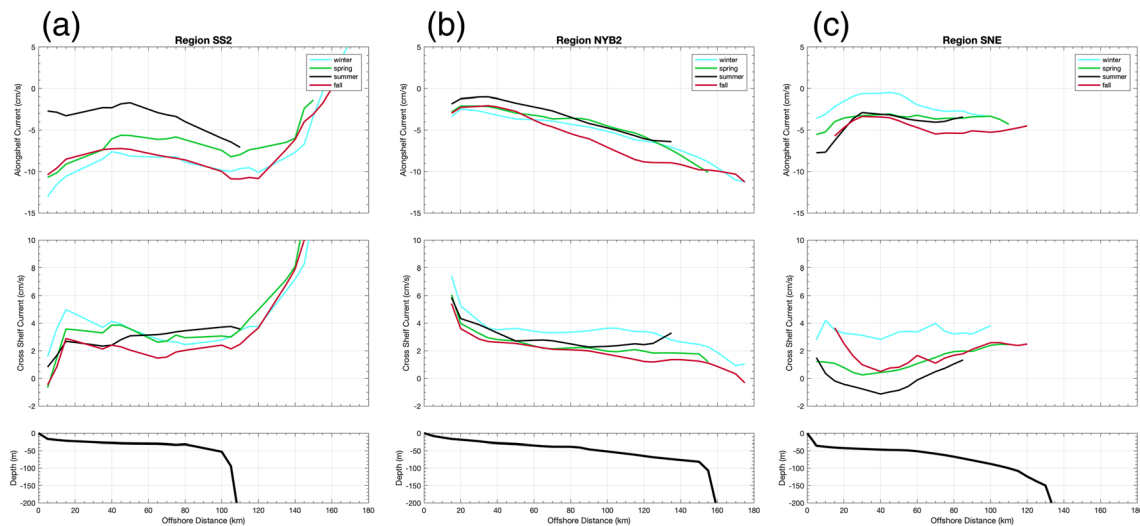


Figure 7. Alongshelf current (top) and cross-shelf current (middle) as a function of distance offshore (km) by season winter (blue), spring (green), summer (black), and fall (red) for three cross sections through MAB: (a) Southern Shelf 2 (SS2), (b) New York Bight 2 (NYB2), and (c) Southern New England (SNE). The bottom panel depicts water depth along each of the three cross sections.

3.5. Seasonal Variability

Next, we examined for each season the variability of the surface flow within the years (intraseasonal variability) and the variability between the years (interseasonal variability). Intraseasonal variability (Figure 8) is found by calculating the standard deviation of the hourly data each season and then averaging the results for all 10 years so that each year is equally weighted. This provides a measure of the short-term variability expected within a season. Interseasonal variability (Figure 9) is calculated by taking the standard deviation of the 10 annual averages. This provides a measure of the year-to-year variability in the seasonal averages.

For the intraseasonal statistics, summer is the least variable with a standard deviation of 11.9 cm/s averaged over the entire field. Winter and fall exhibit the highest variability at 15.4 cm/s. Spring is in between at 14.5 cm/s. Comparing Figure 8 with Figure 4, the standard deviation of the short-term variability is greater than the mean flow speeds. The variability decreases with higher latitude in each of the seasons. Winter, spring, and fall all display less variability over the HSV. As noted by Gong et al. (2010), the spatial variability of the surface currents is affected by different forcing mechanisms at different scales. Wind forcing and stratification operate at shelf wide scales while topography can influence the flow on scales of tens of kilometers.

The interseasonal variability is one third the value of the intraseasonal, implying that the seasonal averages are relatively stable from year to year. For the interseasonal statistics, again, summer is the least variable with a standard deviation of 3.5 cm/s for the whole field. The most significant year-to-year variability in the domain occurs in the southern half of the MAB, either along the shelfbreak jet or along on the southern MAB shelf itself, where the strong currents turn toward the shelfbreak and the Gulf Stream. The variability between summers is high near the eastern side of LIS, which match the findings of Ullman and Codiga (2004), who found a surface-intensified jet that is strongest in the summer and essentially absent in winter. The variability is high between springs at the shelfbreak near 40°N, 71°W, an area where Gulf Stream warm core rings are known to impact the shelf (Zhang & Gawarkiewicz, 2015). The variability between seasons is relatively constant at 3 cm/s along the New Jersey and New York coast. The fall is unique in having both high interseasonal and intraseasonal variability. We will focus on the variability associated with this season in section 4.

4. Discussion

4.1. General Overview: Variability of Surface Circulation in MAB

A 10-year time series of surface ocean currents mapped with a long-range HFR network identified important patterns and pathways in the mean and variance of the surface flow over annual and seasonal time scales.

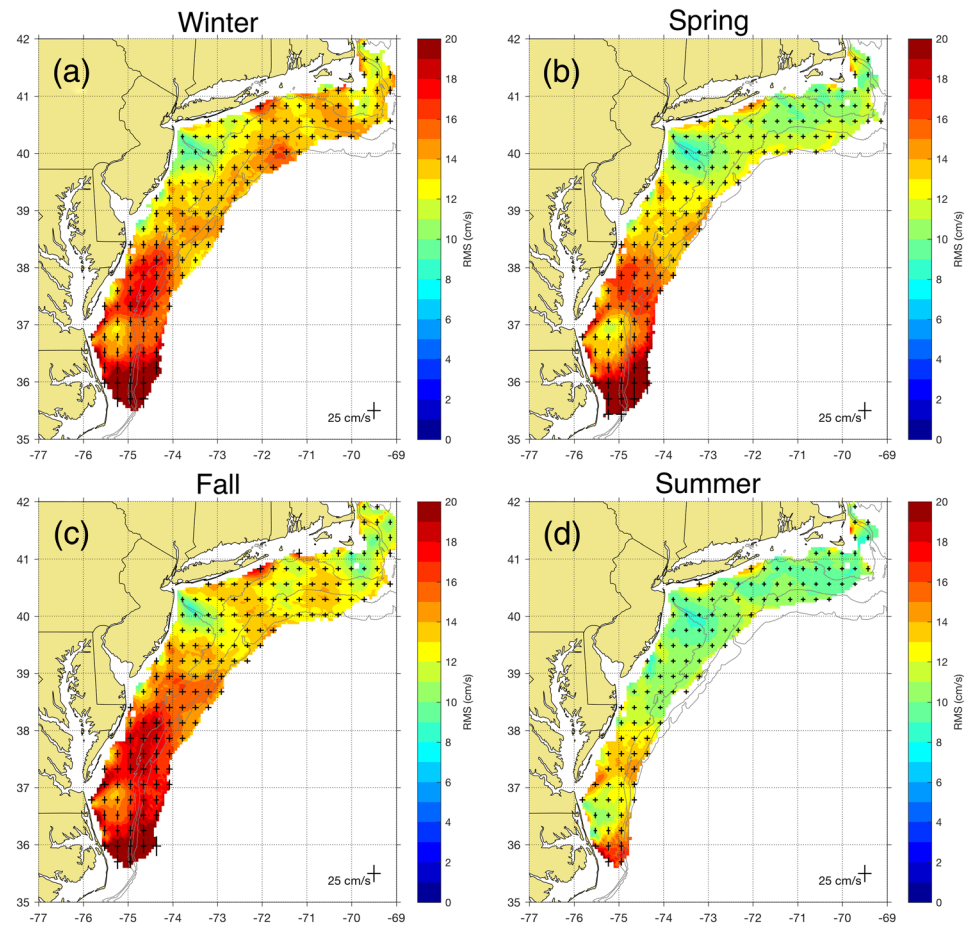


Figure 8. Intraseasonal standard deviation of the surface current (cm/s) in the Mid-Atlantic from (a) winter, December–February; (b) spring, March–May; (c) fall, September–November; and (d) summer, June–August. One standard deviation marks in the east/west and north/south directions are shown for every fifth grid point (30-km spacing) with a reference scale of 25 cm/s in the lower right.

These data show that the variability in the flow over these time scales is twice the magnitude of the mean, driven by similar variance in the local winds. The largest variability in the surface currents was typically seen in the fall and winter seasons when the MAB transitions from a highly stratified water column to a well-mixed water column. During these seasons, energetic wind events and buoyancy inputs drive the observed variability.

The seasonally averaged winds and the variabilities of the winds for the MAB are shown in Figure 3. Autumn and winter generally exhibit stronger winds in the cross-shore direction from the northwest, with more spatial variability in the autumn when the winds are slightly weaker. Progressing from spring into summer, the weaker winds are more alongshore from the southwest, with more spatial variability in the weaker spring. Freshwater input can also be divided into two types of response but offset in time from the winds. Freshwater input is typically largest in winter and spring and lowest in summer and fall. In fall and winter, cross-shore winds are dominant with low riverine flow in the fall and high flow in the winter. On the other hand, spring and summer seasons exhibit predominately alongshore winds with high riverine flow in the spring and low flow in the summer.

The seasonal mean currents from Figure 4 indicate that fall and winter currents are very similar, with the weakest currents inshore in the northern half of the MAB and the highest flows near the shelfbreak and across the entire shelf in the southern MAB. In winter, the spatially consistent strong winds from the northwest may act to diminish the westward alongshore component of flow in the northern MAB. This is quite different from the southern MAB where the relative angle of the wind and shelf geometry is close to

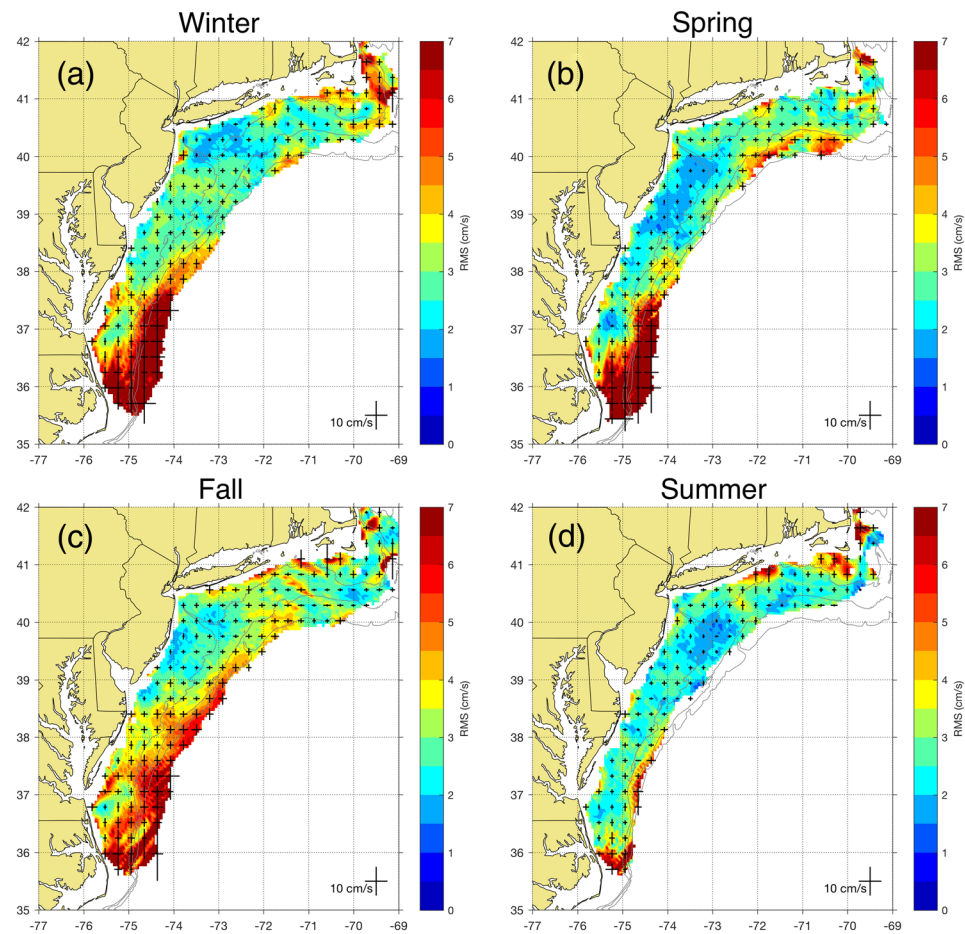


Figure 9. Interseasonal standard deviation of the surface current (cm/s) in the Mid-Atlantic from (a) winter, December–February; (b) spring, March–May; (c) fall, September–November; and (d) summer, June–August. One standard deviation marks in the east/west and north/south directions are shown for every fifth grid point (30-km spacing) with a reference scale of 10 cm/s in the lower right.

orthogonal and the alongshore transport is enhanced by winds in the fall. During this transition season, the flow is directed more alongshore. Spring and summer currents are similar in that both have weaker currents nearshore along the entire MAB, increasing in magnitude with distance offshore, with the strongest currents near the shelfbreak. The cross-shelf pathways are prominent in both the high-flow spring and the low-flow summer. During the high-flow spring, the currents reach speeds similar to the wind driven currents of fall and winter despite having very little average wind forcing.

In general, moving from north to south along the midshelf line with the main current, the alongshore current speeds increase, peaking in Region 4 SS2 (Figure 6a). The alongshore current rapidly increases as the strong current turns offshore and exits the shelf over a seasonally variable 150- to 200-km-wide region. Alongshore currents in the spring and summer are similar with the wind opposing the flow. Fall and winter have the largest alongshore currents, when the wind is cross-shore and the water column is generally less stratified. The alongshore flow is strengthened in the southern MAB in the fall and winter where there is a rotation in the wind to align with alongshore toward the south. Alongshore currents in the winter are the lowest in the northern MAB where they are opposed by the local wind (Figure 7, top right). At midshelf, cross-shelf currents are nearly 2–4 cm/s over much of the MAB. Local peaks in the cross-shelf flow occur at LIS, HSV, and DB (Figure 6b).

Intraseasonal variability is similarly large in fall (high winds speeds) through winter (medium wind speeds and medium river flow) and into spring (low winds and high river flow), with significantly lower variability in the summer. Spring variability is smaller in the northern half of the MAB when winds are very low and

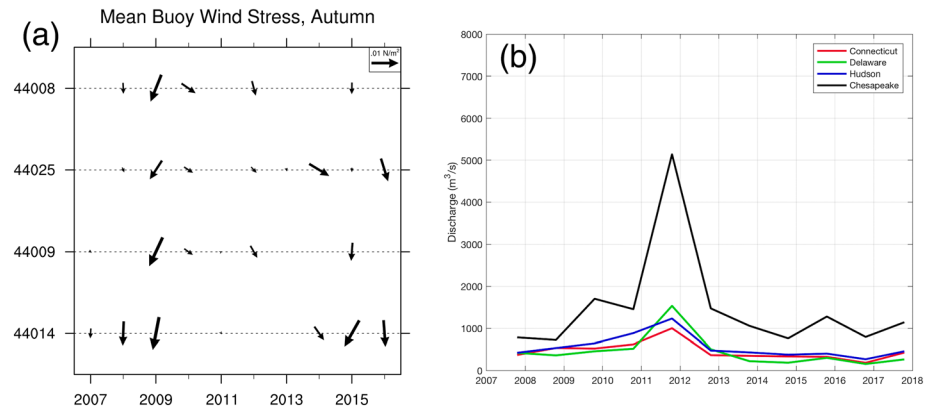


Figure 10. (a) Mean wind stress from the four NDBC buoys in the fall season by year. (b) River discharge from four major rivers/estuaries for the fall season by year: Connecticut (red), Delaware (green), Hudson (blue), and Chesapeake (black).

the rivers have not had their influence. In the southern MAB, the variability during the high-flow season from the Chesapeake is similar to the variability during the fall and winter.

Interseasonal variability shows that the year-to-year variation is greatest in the southern MAB offshore in the outflow region. The observation that the mean and variable currents increase to the south can be explained by the converging isobaths and barotropic flows will be steered along contours of constant f/H , where f is the Coriolis parameter and H represents ocean depth; therefore, the flow will accelerate. Most of the year-to-year variability in the rest of the MAB is near the outer and inner edges of the shelf. Away from the outflow region, the fall has the largest variability, extending across the entire shelf. We therefore chose to look at the variability in the wind forcing and buoyancy inputs during the fall when we expect to see the most implications for shelf wide- differences.

4.2. Detailed Case Study: A Tale of Two Falls

The fall seasonal average wind velocity is plotted for the four main NDBC buoys in Figure 10a. The years 2009 and 2011 stand out as being different from the rest. For the fall 2009 season the winds are the strongest with little spatial variability over the entire MAB. The fall of 2009 was an anomalous wind year in that the winds were stronger and shifted clockwise to be more from the northeast rather than from the northwest typically observed in the fall. This was due in large part to the passage of seven coastal low-pressure systems through the MAB including the extratropical system Nor'Ida (Olabarrieta et al., 2012). The passage of each of these systems stalled in the bight apex, which allowed for the counterclockwise flow around the cyclone to drive surface winds and, consequently surface currents, down the shelf (Figure 11a). The surface currents were aligned toward the southwest with weak cross-shelf transport south of the bight apex.

The fall of 2011 was another anomalous fall for a different reason. This season had the weakest winds between the two buoys that reported. In 2011 there was a large amount of freshwater discharge due to the passage of Hurricane Irene (Glenn et al., 2016) and Tropical Storm Lee (Munroe et al., 2013). These weather systems delivered three times the typical seasonal rainfall (Figure 12) and hence discharge to the northern half of the region as evidenced by the discharge from the Connecticut, Delaware, and Hudson Rivers. These storm systems made an even greater impact on the southern region of the domain by delivering five times the normal fall precipitation and discharge onto the shelf as measured by the discharge from the Chesapeake gauges (Figure 10b). The outflow from rivers is relatively steady, but if an anomalous discharge like that of 2011 occurs, the ocean response is seen across the entire shelf. The response of the currents on the shelf to this increased discharge can be seen as a pronounced offshore surface transport near the exits of the four major estuaries with lower offshore transport between these pathways (Figure 11b).

In order to evaluate overarching meteorological conditions which may be influencing this interannual variability we saw in 2009 and 2011, the synoptic weather types for each fall during the 10-year period were examined using a synoptic typing data set (Siegert et al., 2017; Suriano & Leathers, 2017). Synoptic typing

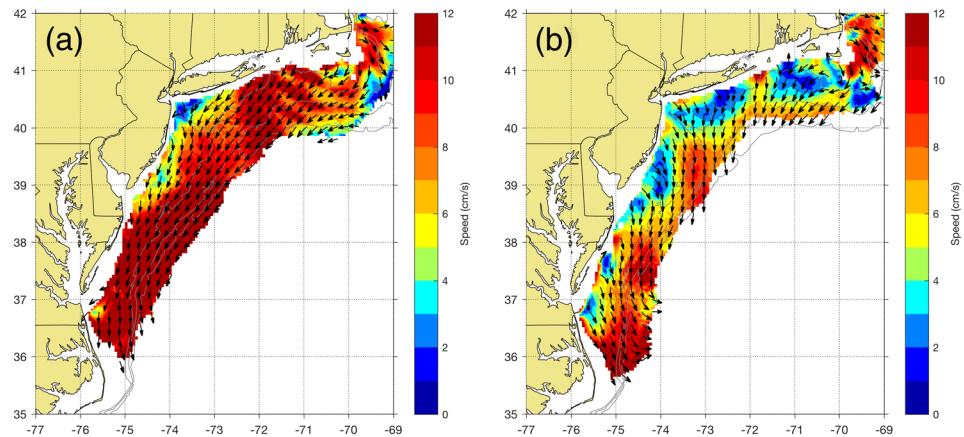


Figure 11. Mean surface currents during the fall, September to November, of (a) 2009 and (b) 2011. Colorbar indicates magnitude (cm/s) and vectors indicate direction toward of surface current.

aims to quantify common features in the daily synoptic weather conditions in order to identify days that are similar using daily surface observations and spatial NCEP/NCAR daily reanalysis data (Kalnay et al., 1996). This synoptic typing data set has been used to evaluate hydroclimatology in the Mid-Atlantic (Siegert et al., 2017), snowfall in the Great Lakes region (Suriano & Leathers, 2017), wind ramp events in the MAB (Veron et al., 2018), and high ozone pollution events in Delaware (Archer et al., 2019), showing broad applicability to weather-related studies throughout the region.

We examined the daily distribution of synoptic types for the fall season (September/October/November 2007–2016), covering the 10 years of the HF radar record. From this analysis, the synoptic type classified as having a strong high-pressure center over New England (spatial average in Figure 13b) emerged as the most prevalent synoptic type during fall 2009, with 26 occurrences out of 92 days in the season, more than any other year in the 10-year period. The New England High is centered overland to the north of the region, producing large-scale winds from the northeast over the MAB. Additionally, several of these days included a

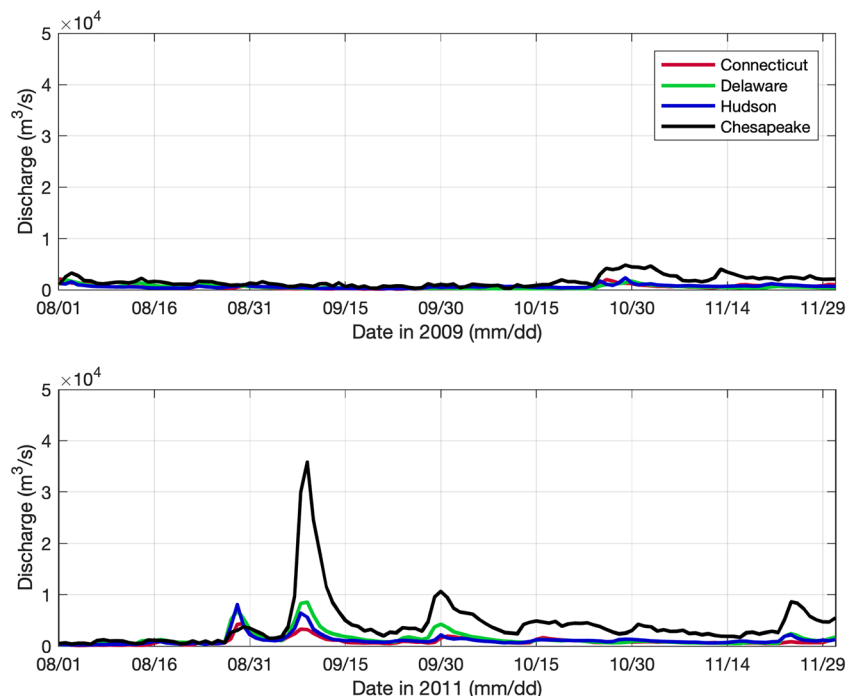


Figure 12. Time series plot of river discharge from four major rivers/estuaries for the fall of 2009 (top) and 2011 (bottom): Connecticut (red), Delaware (green), Hudson (blue), and Chesapeake (black).

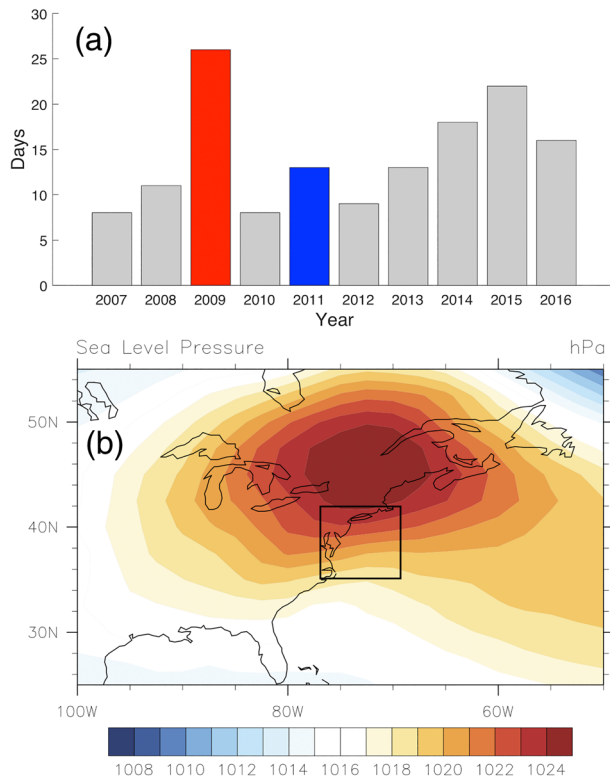


Figure 13. New England High synoptic type classification for the period 2007–2016 where (a) shows the annual distribution of the synoptic type identified in the fall months (September/October/November). The 2009 year is highlighted in red, and the 2011 year is highlighted in blue. (b) The average map of sea level pressure from NCEP/NCAR reanalysis based on all days in the full synoptic data set (1946–2015) for New England high pressure center (type 4,010).

coastal low pressure over the South Atlantic Bight, further reinforcing this onshore wind flow pattern. This indicates that the overall flow pattern over the MAB was likely dominated by both the New England High and earlier discussed coastal storms (Olabarrieta et al., 2012), helping to explain the strong average wind from the northeast seen in Figure 10a during 2009. However, 2011 (Figure 13a, blue bar) has a more typical occurrence of the New England High, and so the river discharge and buoyancy forcing would likely be more important forcing factors to help explain the surface current response in the fall of 2011. The events responsible for the high river discharge anomaly experienced in 2011 are compared to 2009 in Figure 12. River discharge for 2009 is low and steady over the entire fall. In contrast, river discharge in 2011 shows the impact of several storms, including two named tropical storms (Irene & Lee) and additional northeasters. Tropical storms like Irene transited the MAB in less than 12 hr, but the increase in river discharge from the tropical storm rains can last for days.

The fall seasonally averaged surface current maps are compared for 2009 and 2011 in Figure 11. The fall 2009 currents (Figure 11a) are strong across the entire shelf, running alongshelf in nearly the same direction as the wind until reaching the southern MAB where the current turns more offshore. In the fall of 2011 (Figure 11b), currents are weak over the inner shelf, and stronger over the outer shelf, with an offshore component nearly equal to the downshelf component. Unlike 2009, offshore transport at the shelfbreak is observed along the entire Mid-Atlantic, not just in the far southern region. The strong cross-shelf current regions extend inward nearly to the coast near the four estuaries. In between the four estuaries, the weak inner-shelf currents extend to midshelf. The vastly different surface regimes experienced in 2009 and 2011 point to the possibility that different subsurface regimes are also present. Strong surface currents in the direction of the wind in 2009 are consistent with shallow water

Ekman theory for an unstratified shelf. The large buoyancy inputs from the estuaries in 2011 are expected to enhance stratification, which acts to decouple the surface boundary layer from the bottom boundary layer (Chant et al., 2008).

4.3. Oceanographic and Ecological Implications

The implication of the different forcing on the shelf goes beyond those described in the surface current fields above. As has been stated, the fall season marks a significant transition in the MAB as it shifts from a strongly stratified two-layer system to a well-mixed homogenized water column. Using autonomous underwater glider sections along the Endurance Line from Tuckerton, NJ, to the shelfbreak (Castelao et al., 2008), we describe the oceanographic implications on the shelf hydrography (Figure 14). A glider deployed in the fall of 2009 as part of an Observing System Simulation Experiment (Schofield et al., 2010; Wang et al., 2013) indicates that the surface was cool (around 18°C; Figure 14a) with relatively high salinity nearshore (Figure 14c). The water column was well mixed nearshore, and thermocline was at a depth of 40 m. Cross-shelf temperature and salinity sections indicate that the windy 2009 fall transition to well-mixed conditions was nearly complete by mid-November. The core of the cold pool was offshore, starting at the 50-m isobath and extending to the 80-m isobath. The strong winds and resulting surface currents drove strong downwelling throughout the season, pushing the warm surface water up against the coast and forcing the cold pool offshore, resulting in a well-mixed water column on the inner shelf. Upwelling of the cold pool had occurred on the inner side of the stratified zone, with the well-mixed shallow area cutting off access to the coast (Austin & Lentz, 2002). Over much of the continental shelf this year, the wind influence extends to the bottom.

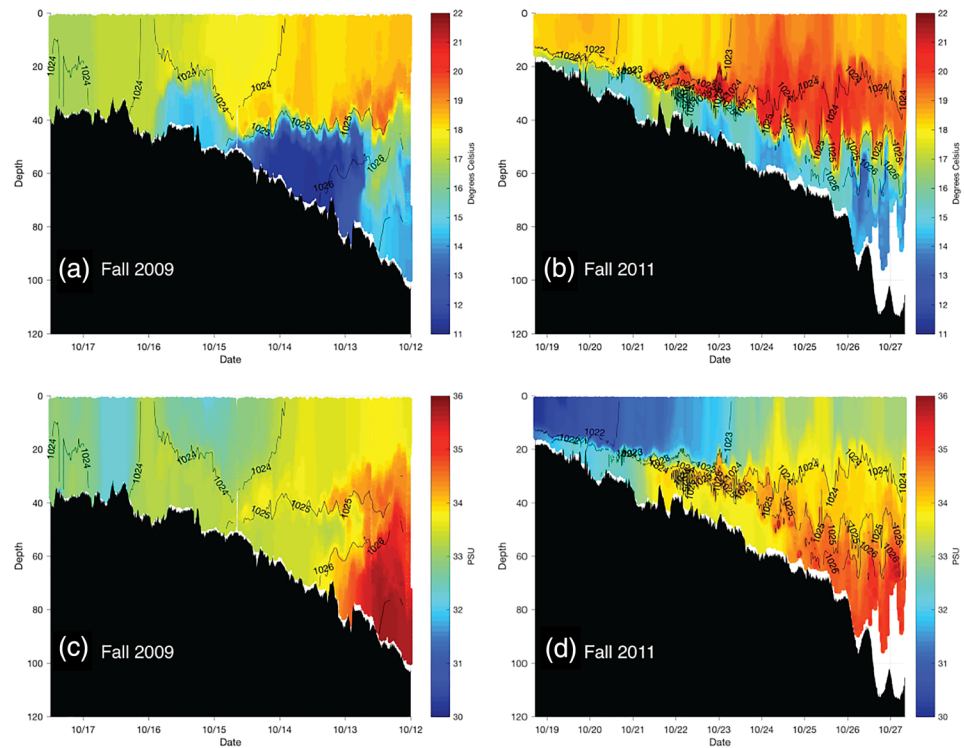


Figure 14. Temperature (top) and salinity (bottom) sections along the Tuckerton Endurance Line offshore of New Jersey for the fall of 2009 (left) and fall of 2011 (right).

In contrast, during the fall of 2011, a glider deployed in support of the Mid-Atlantic Regional Association Coastal Ocean Observing System (MARACOOS) (Brown et al., 2012) indicates that the surface waters were warmer at 20°C (Figure 14b) and the salinity nearshore was much lower (Figure 14d). These lower salinities are the result of much more freshwater discharged from multiple storms including Irene and Lee that moved through the area. The stratification was much stronger in 2011 with the thermocline present over the entire shelf with a depth of 20 m nearshore deepening to 40 m offshore. This intense MAB temperature and salinity stratification persisted at least through late November. This cross-shelf section indicates that the cold pool extended across the entire shelf, even inshore of the 20-m isobath. The strong stratification results in what Chant et al. (2008) characterize as a more slippery interface between the surface and bottom layers, working to decouple the surface layer response from the influence of the bottom. In the fall of 2011, the wind influence is confined to the surface layer over this glider section, while the bottom layer response is dominated by cross and alongshelf pressure gradients.

The 2009 and 2011 fall seasons exemplify the significant variability in the forcing, ocean surface response, and hydrography throughout the water column and across the shelf. Consequently, these physical characteristics have impacts on the marine life in this region. Some 321 species of fish call the MAB home (Able & Fahay, 1998). These species have evolved with seasonal dependent phenologies that anticipate and take advantage of this physical variability. For example, certain flounder species, such as the summer flounder, will time their spawn with the MAB fall transition. Adults two or more years old spawn as they migrate in September through November (Wilk et al., 1980). Their larvae are neutrally buoyant and adrift at the surface for 30 days. Therefore, the connection between summer flounder spawning grounds and nursery grounds is based upon the transport of larvae in the fall. Given the observed currents in our 10-year data set, the transport of these larvae and their success to recruit into the fishery depend on the local forcing (Brodziak & O'Brien, 2005). In 2009, when the alongshore currents were strong and to the southwest, these larvae were rapidly advected south. In 2011, when significant freshwater outflow lead to a more cross-shore transport pathway, the larvae likely moved offshore much faster than down the shelf.

5. Conclusion

Surface current patterns on the MAB's broad seasonally stratified continental shelf are highly influenced by variability in the wind field and the riverine inflow of fresh water. This study used a decade of hourly surface current maps from an HFR network that spans the full MAB combined with wind observations from meteorological buoys and coastal stations as well as river discharges from the national stream gauge network. Ten-year annual and seasonal means, along with their interannual and intra-annual variability, were calculated to study the spatial patterns of the mean surface currents and their relation to the mean wind and riverine forcing.

Generally, the 10-year annual mean surface currents are (a) offshore and weaker, about 3–6 cm/s, near the coast; (b) increase in speed to about 8–10 cm/s and rotate to an alongshore direction on the outer shelf; and (c) similarly increase in speed and rotate to flow offshore toward the Gulf Stream in the southern MAB. The year-to-year interannual variability is low, with a standard deviation of about 1–3 cm/s over most of the shelf, but the variability within a year is much greater, with a typical standard deviation of 10–20 cm/s over the same region.

Compared to the annual mean, the four 10-year seasonal mean surface current maps generally exhibit similar spatial patterns but with different current magnitudes and slightly different directions, with winter and summer more cross-shore and the transition seasons of fall and spring more alongshore. Fall and winter, with their strong cross-shore mean winds, have the strongest mean currents, while summer, with its opposing alongshore mean winds, has the weakest mean currents. Again, compared to the seasonal means, the seasonal interannual variability is lower, and the seasonal intra-annual variability is higher.

The season with the most variability was the fall, when the MAB transitions from highly stratified summer conditions to well-mixed winter conditions. Examination of the annual wind and river discharge records indicates that fall of 2009 experienced an anomalously strong and coherent wind field over the MAB, while the fall of 2011 had anomalously high river discharges due to a series of tropical and extratropical rainstorms. The spatial patterns of surface currents for these two fall seasons are different, with the relatively windy dry fall of 2009 exhibiting strong (8–10 cm/s) alongshore currents to the southwest over the entire MAB, while the low wind but rainy fall of 2011 exhibited weak (1–4 cm/s) cross-shelf currents over much of the inner shelf with cross-shelf peaks near the rivers. Cross-shelf temperature and salinity sections indicate that the windy 2009 fall transition to well-mixed conditions was nearly complete by mid-November, but that in the wet fall of 2011, the intense MAB temperature and salinity stratification persisted at least through late November.

The MAB is the southern half of the Northeast U.S. Large Marine Ecosystem (LME). Long-term surface current observations, especially over seasonal time scales, provide insights into the physical conditions organisms have adapted to in these productive waters. Larvae that are neutrally buoyant are advected by these currents. Temperature sensitive fish migrate across-shelf based on the timing of the seasonal transitions. The MAB is also a densely populated urbanized coast that supports multiple human activities, including fishing, marine transportation, and a developing offshore wind energy industry. Improved understanding of the mean currents and their variability will enable more informed development, better management of pollutants, and response to events, both natural and human made.

Data Availability Statement

Data sets for this research are available in these in-text data citation reference: Roarty (2020), (Creative Commons Attribution 4.0 International).

References

- Able, K. W., & Fahay, M. P. (1998). *The first year in the life of estuarine fishes in the Middle Atlantic Bight*. New Jersey: Rutgers University Press New Brunswick.
- Andres, M. (2016). On the recent destabilization of the Gulf Stream path downstream of Cape Hatteras. *Geophysical Research Letters*, *43*, 9836–9842. <https://doi.org/10.1002/2016GL069966>
- Archer, C. L., Brodie, J. F., & Rauscher, S. A. (2019). Global warming will aggravate ozone pollution in the US Mid-Atlantic. *Journal of Applied Meteorology and Climatology*, *58*(6), 1267–1278. <https://doi.org/10.1175/JAMC-D-18-0263.1>
- Austin, J. A., & Lentz, S. J. (2002). The inner shelf response to wind-driven upwelling and downwelling. *Journal of Physical Oceanography*, *32*(7), 2171–2193. [https://doi.org/10.1175/1520-0485\(2002\)032<2171:TISRTW>2.0.CO;2](https://doi.org/10.1175/1520-0485(2002)032<2171:TISRTW>2.0.CO;2)

Acknowledgments

The authors would like to recognize the effort of the technical team that kept the radar stations operating during this 10-year period that included Rich Arena, Chris Jakubiak, Zhitao Yu, and Colin Evans. The MARACOOS HFR network was supported from 2007–2010 by NOAA Award Number NA07NOS4730221 “Phased Deployment and Operation of the Mid-Atlantic Regional Coastal Ocean Observing System (MARCOOS)” and from 2011–2016 by NOAA Award Number NA11NOS0120038 “Towards a Comprehensive Mid-Atlantic Regional Association Coastal Ocean Observing System (MARACOOS).” Sponsor: National Ocean Service (NOS), National Oceanic and Atmospheric Administration (NOAA) NOAA-NOS-IOOS-2011-2002515/CFDA: 11.012, Integrated Ocean Observing System Topic Area 1: Continued Development of Regional Coastal Ocean Observing Systems. The MARACOOS HFR network was supported from 2016–2021 by NOAA Award Number NOAA-NOS-IOOS-2016-2004378 “MARACOOS: Preparing for a Changing Mid-Atlantic.”

- Beardsley, R., & Winant, C. (1979). On the mean circulation in the Mid-Atlantic Bight. *Journal of Physical Oceanography*, 9(3), 612–619. [https://doi.org/10.1175/1520-0485\(1979\)009<0612:OTMCIT>2.0.CO;2](https://doi.org/10.1175/1520-0485(1979)009<0612:OTMCIT>2.0.CO;2)
- Beardsley, R. C., & Boicourt, W. C. (1981). On estuarine and continental-shelf circulation in the Middle Atlantic Bight. In B. A. Warren & C. Wunsch (Eds.), *Evolution of Physical Oceanography: Scientific Surveys in Honor of Henry Stommel* (Vol. 1, pp. 198–233). Cambridge, MA: MIT Press.
- Beardsley, R. C., Boicourt, W., & Hansen, D. (1976). Current variability and mean circulation in Middle Atlantic Bight. In *Transactions American Geophysical Union* (Vol. 57, pp. 262–262). Washington DC: American Geophysical Union.
- Beardsley, R. C., Chapman, D. C., Brink, K. H., Ramp, S. R., & Schlitz, R. (1985). The Nantucket Shoals Flux Experiment (NSFE79). Part I: A basic description of the current and temperature variability. *Journal of Physical Oceanography*, 15(6), 713–748. [https://doi.org/10.1175/1520-0485\(1985\)015<0713:TNSFEP>2.0.CO;2](https://doi.org/10.1175/1520-0485(1985)015<0713:TNSFEP>2.0.CO;2)
- Beardsley, R. C., & Haidvogel, D. B. (1981). Model studies of the wind-driven transient circulation in the Middle Atlantic Bight. Part 1: Adiabatic boundary conditions. *Journal of Physical Oceanography*, 11(3), 355–375. [https://doi.org/10.1175/1520-0485\(1981\)011<0355:MSOTWD>2.0.CO;2](https://doi.org/10.1175/1520-0485(1981)011<0355:MSOTWD>2.0.CO;2)
- Bigelow, H. B., & Sears, M. (1935). Studies of the waters on the continental shelf, Cape Cod to Chesapeake Bay. II. Salinity. *Papers in Physical Oceanography and Meteorology*, 4, 94.
- Brodziak, J., & O'Brien, L. (2005). Do environmental factors affect recruits per spawner anomalies of New England groundfish? *ICES Journal of Marine Science*, 62(7), 1394–1407. <https://doi.org/10.1016/j.icesjms.2005.04.019>
- Brown, W., Boicourt, W., Flagg, C., Gangopadhyay, A., Schofield, O., Glenn, S., & Kohut, J. (2012). Mapping the Mid-Atlantic Cold Pool evolution and variability with ocean gliders and numerical models. *2012 Oceans*. <https://doi.org/10.1109/oceans.2012.6404970>
- Bumpus, D. F. (1969). Reversals in surface drift in Middle Atlantic Bight area. *Deep-Sea Research*, 17–23.
- Castelao, R., Glenn, S., Schofield, O., Chant, R., Wilkin, J., & Kohut, J. (2008). Seasonal evolution of hydrographic fields in the central Middle Atlantic Bight from glider observations. *Geophysical Research Letters*, 35, L03617. <https://doi.org/10.1029/2007GL032335>
- Chant, R. J., Glenn, S. M., Hunter, E., Kohut, J., Chen, R. F., Houghton, R. W., et al. (2008). Bulge formation of a buoyant river outflow. *Journal of Geophysical Research*, 113, C01017. <https://doi.org/10.1029/2007JC004100>
- Chapman, D. C., & Beardsley, R. C. (1989). On the origin of shelf water in the Middle Atlantic Bight. *Journal of Physical Oceanography*, 19(3), 384–391. [https://doi.org/10.1175/1520-0485\(1989\)019<0384:OTOOSW>2.0.CO;2](https://doi.org/10.1175/1520-0485(1989)019<0384:OTOOSW>2.0.CO;2)
- Chen, C., Beardsley, R. C., & Limeburner, R. (1995). Variability of currents in late spring in the northern Great South Channel. *Continental Shelf Research*, 15(4–5), 451–473. [https://doi.org/10.1016/0278-4343\(94\)00056-S](https://doi.org/10.1016/0278-4343(94)00056-S)
- Dzwonkowski, B., Kohut, J. T., & Yan, X.-H. (2009). Seasonal differences in wind-driven across-shelf forcing and response relationships in the shelf surface layer of the central Mid-Atlantic Bight. *Journal of Geophysical Research*, 114, C08018. <https://doi.org/10.1029/2008JC004888>
- Dzwonkowski, B., Lipphardt, B. L. Jr., Kohut, J. T., Yan, X.-H., & Garvine, R. W. (2010). Synoptic measurements of episodic offshore flow events in the central Mid-Atlantic Bight. *Continental Shelf Research*, 30(12), 1373–1386. <https://doi.org/10.1016/j.csr.2010.05.004>
- Flagg, C. N., Dunn, M., Wang, D. P., Rossby, H. T., & Benway, R. L. (2006). A study of the currents of the outer shelf and upper slope from a decade of shipboard ADCP observations in the Middle Atlantic Bight. *Journal of Geophysical Research*, 111, C06003. <https://doi.org/10.1029/2005JC003116>
- Fleming, N. E. (2016). *Seasonal and spatial variability in temperature, salinity and circulation of the Middle Atlantic Bight*, PhD Thesis. Rutgers: The State University of New Jersey-New Brunswick.
- Fratantoni, P., & Pickart, R. (2003). Variability of the shelf break jet in the Middle Atlantic Bight: Internally or externally forced? *Journal of Geophysical Research*, 108(C5), 3166. <https://doi.org/10.1029/2002JC001326>
- Frey, H. R. (1978). Northeastward drift in the Northern Mid-Atlantic bight during late spring and summer 1976. *Journal of Geophysical Research*, 83(C1), 503–504. <https://doi.org/10.1029/JC083iC01p00503>
- Glenn, S., Miles, T., Seroka, G., Xu, Y., Forney, R., Yu, F., et al. (2016). Stratified coastal ocean interactions with tropical cyclones. *Nature Communications*, 7(1), 10887. <https://doi.org/10.1038/ncomms10887>
- Gong, D., Kohut, J. T., & Glenn, S. M. (2010). Seasonal climatology of wind-driven circulation on the New Jersey Shelf. *Journal of Geophysical Research*, 115, C04006. <https://doi.org/10.1029/2009JC005520>
- Greene, C. A., Thirumalai, K., Kearney, K. A., Delgado, J. M., Schwanghart, W., Wolfenbarger, N. S., et al. (2019). The climate data toolbox for MATLAB. *Geochemistry, Geophysics, Geosystems*, 20, 3774–3781. <https://doi.org/10.1029/2019GC008392>
- Haines, S., Seim, H., & Muglia, M. (2017). Implementing quality control of high-frequency radar estimates and application to Gulf Stream surface currents. *Journal of Atmospheric and Oceanic Technology*, 34(6), 1207–1224. <https://doi.org/10.1175/JTECH-D-16-0203.1>
- Kalnay, E., Kanamitsu, M., Kistler, R., Collins, W., Deaven, D., Gandin, L., et al. (1996). The NCEP/NCAR 40-year reanalysis project. *Bulletin of the American Meteorological Society*, 77(3), 437–471. [https://doi.org/10.1175/1520-0477\(1996\)077<0437:TNYRP>2.0.CO;2](https://doi.org/10.1175/1520-0477(1996)077<0437:TNYRP>2.0.CO;2)
- Kim, S. Y., Terrill, E. J., & Cornuelle, B. D. (2008). Mapping surface currents from HF radar radial velocity measurements using optimal interpolation. *Journal of Geophysical Research*, 113, C10023. <https://doi.org/10.1029/2007JC004244>
- Kohut, J., Roarty, H., Randall-Goodwin, E., Glenn, S., & Lichtenwalner, C. (2012). Evaluation of two algorithms for a network of coastal HF radars in the Mid-Atlantic Bight. *Ocean Dynamics*, 62(6), 953–968. <https://doi.org/10.1007/s10236-012-0533-9>
- Kohut, J. T., & Glenn, S. M. (2003). Improving HF radar surface current measurements with measured antenna beam patterns. *Journal of Atmospheric and Oceanic Technology*, 20(9), 1303–1316. [https://doi.org/10.1175/1520-0426\(2003\)020<1303:IHRSCM>2.0.CO;2](https://doi.org/10.1175/1520-0426(2003)020<1303:IHRSCM>2.0.CO;2)
- Kohut, J. T., Glenn, S. M., & Chant, R. J. (2004). Seasonal current variability on the New Jersey inner shelf. *Journal of Geophysical Research*, 109, C07S07. <https://doi.org/10.1029/2003JC001963>
- Kohut, J. T., Glenn, S. M., & Paduan, J. D. (2006). Inner shelf response to Tropical Storm Floyd. *Journal of Geophysical Research*, 111, C09S91. <https://doi.org/10.1029/2003JC002173>
- Kohut, J. T., Roarty, H. J., & Glenn, S. M. (2006). Characterizing observed environmental variability with HF Doppler radar surface current mappers and acoustic Doppler current profilers: Environmental variability in the Coastal Ocean. *IEEE Journal of Oceanic Engineering*, 31(4), 876–884. <https://doi.org/10.1109/JOE.2006.886095>
- Lentz, S. J. (2008). Observations and a model of the mean circulation over the Middle Atlantic Bight Continental Shelf. *Journal of Physical Oceanography*, 38(6), 1203–1221. <https://doi.org/10.1175/2007JPO3768.1>
- Lentz, S. J., Butman, B., & Harris, C. (2014). The vertical structure of the circulation and dynamics in Hudson Shelf Valley. *Journal of Geophysical Research: Oceans*, 119, 3694–3713. <https://doi.org/10.1002/2014JC009883>
- Lentz, S. J., Elgar, S., & Guza, R. (2003). Observations of the flow field near the nose of a buoyant coastal current. *Journal of Physical Oceanography*, 33(4), 933–943. [https://doi.org/10.1175/1520-0485\(2003\)33<933:OOTFFN>2.0.CO;2](https://doi.org/10.1175/1520-0485(2003)33<933:OOTFFN>2.0.CO;2)

- Levin, J., Wilkin, J., Fleming, N., & Zavala-Garay, J. (2018). Mean circulation of the Mid-Atlantic Bight from a climatological data assimilative model. *Ocean Modelling*, *128*, 1–14. <https://doi.org/10.1016/j.ocemod.2018.05.003>
- Limeburner, R., & Beardsley, R. C. (1982). The seasonal hydrography and circulation over Nantucket Shoals. *Journal of Marine Research*, *40*, 371–406.
- Linder, C. A., & Gawarkiewicz, G. (1998). A climatology of the shelfbreak front in the Middle Atlantic Bight. *Journal of Geophysical Research*, *103*(C9), 18,405–18,423. <https://doi.org/10.1029/98JC01438>
- Miller, A. R. (1952). *A pattern of surface coastal circulation inferred from surface salinity-temperature data and drift bottle recoveries*, WHOI Tech. Rep. 52–28. Woods Hole, Massachusetts: Woods Hole Oceanographic Institution. 14 pp
- Moore, C. N., Fernandez-Partagas, J., & Price, J. F. (1976). *Meteorological forcing fields of the New York Bight (first year's progress report)*, Tech. Rep. TR76–8. Miami Florida: Rosenstiel School of Marine and Atmospheric Science.
- Mountain, D. G. (2003). Variability in the properties of shelf water in the Middle Atlantic Bight, 1977–1999. *Journal of Geophysical Research*, *108*(C1), 3014. <https://doi.org/10.1029/2001JC001044>
- Munroe, D., Tabatabai, A., Burt, L., Bushek, D., Powell, E. N., & Wilkin, J. (2013). Oyster mortality in Delaware Bay: Impacts and recovery from Hurricane Irene and Tropical Storm Lee. *Estuarine, Coastal and Shelf Science*, *135*, 209–219. <https://doi.org/10.1016/j.ecss.2013.10.011>
- Olabarrieta, M., Warner, J. C., Armstrong, B., Zambon, J. B., & He, R. (2012). Ocean-atmosphere dynamics during Hurricane Ida and Nor'Ida: An application of the coupled ocean-atmosphere-wave-sediment transport (COAWST) modeling system. *Ocean Modelling*, *43*, 112–137. <https://doi.org/10.1016/j.ocemod.2011.12.008>
- Ou, H. W., Beardsley, R. C., Mayer, D., Boicourt, W. C., & Butman, B. (1981). An analysis of subtidal current fluctuations in the Middle Atlantic Bight. *Journal of Physical Oceanography*, *11*(10), 1383–1392. [https://doi.org/10.1175/1520-0485\(1981\)011<1383:AAOSCF>2.0.CO;2](https://doi.org/10.1175/1520-0485(1981)011<1383:AAOSCF>2.0.CO;2)
- Paduan, J. D., & Graber, H. C. (1997). Introduction to high-frequency radar: Reality and myth. *Oceanography*, *10*(2), 36–39. <https://doi.org/10.5670/oceanog.1997.18>
- Pawlowicz, R., Beardsley, B., & Lentz, S. (2002). Classical tidal harmonic analysis including error estimates in MATLAB using T_TIDE. *Computers & Geosciences*, *28*(8), 929–937. [https://doi.org/10.1016/S0098-3004\(02\)00013-4](https://doi.org/10.1016/S0098-3004(02)00013-4)
- Pringle, J. M. (2018). Remote forcing of shelf flows by density gradients and the origin of the annual mean flow on the Mid-Atlantic Bight. *Journal of Geophysical Research: Oceans*, *123*, 4464–4482. <https://doi.org/10.1029/2017JC013721>
- Roarty, H. J., Glenn, S. M., Kohut, J. T., Gong, D., Handel, E., Rivera Lemus, E., et al. (2010). Operation and application of a regional High Frequency Radar network in the Mid Atlantic Bight. *Marine Technology Society Journal*, *44*(6), 133–145. <https://doi.org/10.4031/MTSJ.44.6.5>
- Roarty, H. (2020). *2007–2016 surface circulation over the Mid Atlantic Bight continental shelf derived from a decade of High Frequency Radar observations (Version 01) [data set]*. Meyrin, Canton of Geneva, Switzerland: Zenodo. <http://doi.org/10.5281/zenodo.3770921>
- Schofield, O., Glenn, S., Orcutt, J., Arrott, M., Meisinger, M., Gangopadhyay, A., et al. (2010). Automated sensor networks to advance ocean science. *Eos, Transactions of the American Geophysical Union*, *91*(39), 345–346. <https://doi.org/10.1029/2010EO390001>
- Siegert, C., Leathers, D., & Levina, D. (2017). Synoptic typing: Interdisciplinary application methods with three practical hydroclimatological examples. *Theoretical and Applied Climatology*, *128*(3–4), 603–621. <https://doi.org/10.1007/s00704-015-1700-y>
- Soulsby, R. L., Hamm, L., Klopman, G., Myrhaug, D., Simons, R. R., & Thomas, G. P. (1993). Wave-current interaction within and outside the bottom boundary layer. *Coastal Engineering*, *21*(1–3), 41–69. [https://doi.org/10.1016/0378-3839\(93\)90045-A](https://doi.org/10.1016/0378-3839(93)90045-A)
- Stewart, R. H., & Joy, J. W. (1974). HF radio measurements of surface currents. In *Deep sea research and oceanographic abstracts* (Vol. 21, pp. 1039–1049). Great Britain: Elsevier. [https://doi.org/10.1016/0011-7471\(74\)90066-7](https://doi.org/10.1016/0011-7471(74)90066-7)
- Suriano, Z. J., & Leathers, D. J. (2017). Synoptic climatology of lake-effect snowfall conditions in the eastern Great Lakes region. *International Journal of Climatology*, *37*(12), 4377–4389. <https://doi.org/10.1002/joc.5093>
- Sverdrup, H. U., Johnson, M. W., & Fleming, R. H. (1942). *The oceans: Their physics, chemistry, and general biology*. New York: Prentice-Hall.
- Terrill, E., Otero, M., Hazard, L., Conlee, D., Harlan, J., Kohut, J., et al. (2006). Data management and real-time distribution in the HF-radar national network. In *OCEANS 2006* (pp. 1–6). Boston, MA: IEEE. <https://ieeexplore.ieee.org/document/4099038>
- Thomson, R. E., & Emery, W. J. (2014). *Data analysis methods in physical oceanography*. Newnes. Waltham, MA: Elsevier B. V.
- Ullman, D. S., & Codiga, D. L. (2004). Seasonal variation of a coastal jet in the Long Island Sound outflow region based on HF radar and Doppler current observations. *Journal of Geophysical Research*, *109*, C07S06. <https://doi.org/10.1029/2002JC001660>
- Ullman, D. S., O'Donnell, J., Kohut, J., Fake, T., & Allen, A. (2006). Trajectory prediction using HF radar surface currents: Monte Carlo simulations of prediction uncertainties. *Journal of Geophysical Research*, *111*, C12005. <https://doi.org/10.1029/2006JC003715>
- Veron, D. E., Brodie, J. F., Shirazi, Y. A., & Gilchrist, J. R. (2018). Modeling the electrical grid impact of wind ramp-up forecasting error offshore in the Mid-Atlantic region. *Journal of Renewable and Sustainable Energy*, *10*(1), 013308. <https://doi.org/10.1063/1.4990684>
- Wallace, E. J., Looney, L. B., & Gong, D. (2018). Multi-decadal trends and variability in temperature and salinity in the Mid-Atlantic Bight, Georges Bank, and Gulf of Maine. *Journal of Marine Research*, *76*, 163–215. <https://doi.org/10.1357/002224018826473281>
- Wang, X., Chao, Y., Thompson, D. R., Chien, S. A., Farrara, J., Li, P., et al. (2013). Multi-model ensemble forecasting and glider path planning in the Mid-Atlantic Bight. *Continental Shelf Research*, *63*, S223–S234. <https://doi.org/10.1016/j.csr.2012.07.006>
- Wilk, S. J., Smith, W. G., Ralph, D. E., & Sibunka, J. (1980). The population structure of summer flounder between New York and Florida based on linear discriminant analysis. *Transactions of the American Fisheries Society*, *109*(3), 265–271. [https://doi.org/10.1577/1548-8659\(1980\)109<265:PSOSFB>2.0.CO;2](https://doi.org/10.1577/1548-8659(1980)109<265:PSOSFB>2.0.CO;2)
- Zhang, W. G., & Gawarkiewicz, G. G. (2015). Dynamics of the direct intrusion of Gulf Stream ring water onto the Mid-Atlantic Bight shelf. *Geophysical Research Letters*, *42*, 7687–7695. <https://doi.org/10.1002/2015GL065530>
- Zhang, W. G., Wilkin, J. L., & Chant, R. J. (2009). Modeling the pathways and mean dynamics of river plume dispersal in the New York Bight. *Journal of Physical Oceanography*, *39*, 1167–1183. <https://doi.org/10.1175/2008JPO4082.1>
- Zhu, J., & Liang, X.-Z. (2013). Impacts of the Bermuda high on regional climate and ozone over the United States. *Journal of Climate*, *26*(3), 1018–1032. <https://doi.org/10.1175/JCLI-D-12-00168.1>